

# Broadband observations of the naked-eye $\gamma$ -ray burst GRB 080319B

J. L. Racusin<sup>1</sup>, S. V. Karpov<sup>2</sup>, M. Sokolowski<sup>3</sup>, J. Granot<sup>4</sup>, X. F. Wu<sup>1,5</sup>, V. Pal'shin<sup>6</sup>, S. Covino<sup>7</sup>, A. J. van der Horst<sup>8</sup>, S. R. Oates<sup>9</sup>, P. Schady<sup>9</sup>, R. J. Smith<sup>10</sup>, J. Cummings<sup>11</sup>, R. L. C. Starling<sup>12</sup>, L. W. Piotrowski<sup>13</sup>, B. Zhang<sup>14</sup>, P. A. Evans<sup>12</sup>, S. T. Holland<sup>15,16,17</sup>, K. Malek<sup>18</sup>, M. T. Page<sup>9</sup>, L. Vetere<sup>1</sup>, R. Margutti<sup>19</sup>, C. Guidorzi<sup>7,10</sup>, A. P. Kamble<sup>20</sup>, P. A. Curran<sup>20</sup>, A. Beardmore<sup>12</sup>, C. Kouveliotou<sup>21</sup>, L. Mankiewicz<sup>18</sup>, A. Melandri<sup>10</sup>, P. T. O'Brien<sup>12</sup>, K. L. Page<sup>12</sup>, T. Piran<sup>22</sup>, N. R. Tanvir<sup>12</sup>, G. Wrochna<sup>3</sup>, R. L. Aptekar<sup>6</sup>, S. Barthelmy<sup>11</sup>, C. Bartolini<sup>23</sup>, G. M. Beskin<sup>2</sup>, S. Bondar<sup>24</sup>, M. Bremer<sup>25</sup>, S. Campana<sup>7</sup>, A. Castro-Tirado<sup>26</sup>, A. Cucchiara<sup>1</sup>, M. Cwiok<sup>13</sup>, P. D'Avanzo<sup>7</sup>, V. D'Elia<sup>27</sup>, M. Della Valle<sup>28,29</sup>, A. de Ugarte Postigo<sup>30</sup>, W. Dominik<sup>13</sup>, A. Falcone<sup>1</sup>, F. Fiore<sup>27</sup>, D. B. Fox<sup>1</sup>, D. D. Frederiks<sup>6</sup>, A. S. Fruchter<sup>31</sup>, D. Fugazza<sup>7</sup>, M. A. Garrett<sup>32,33,34</sup>, N. Gehrels<sup>11</sup>, S. Golenetskii<sup>6</sup>, A. Gomboc<sup>35</sup>, J. Gorosabel<sup>26</sup>, G. Greco<sup>23</sup>, A. Guarnieri<sup>23</sup>, S. Immler<sup>15,17</sup>, M. Jelinek<sup>26</sup>, G. Kasprzyk<sup>36</sup>, V. La Parola<sup>37</sup>, A. J. Levan<sup>38</sup>, V. Mangano<sup>37</sup>, E. P. Mazets<sup>6</sup>, E. Molinari<sup>7</sup>, A. Moretti<sup>7</sup>, K. Nawrocki<sup>3</sup>, P. P. Oleynik<sup>6</sup>, J. P. Osborne<sup>12</sup>, C. Pagani<sup>1</sup>, S. B. Pandey<sup>39</sup>, Z. Paragi<sup>40</sup>, M. Perri<sup>41</sup>, A. Piccioni<sup>23</sup>, E. Ramirez-Ruiz<sup>42</sup>, P. W. A. Roming<sup>1</sup>, I. A. Steele<sup>10</sup>, R. G. Strom<sup>20,32</sup>, V. Testa<sup>27</sup>, G. Tosti<sup>43</sup>, M. V. Ulanov<sup>6</sup>, K. Wiersema<sup>12</sup>, R. A. M. J. Wijers<sup>20</sup>, J. M. Winters<sup>25</sup>, A. F. Zarnecki<sup>13</sup>, F. Zerbi<sup>7</sup>, P. Mészáros<sup>1,44</sup>, G. Chincarini<sup>7,19</sup> & D. N. Burrows<sup>1</sup>

**Long-duration  $\gamma$ -ray bursts (GRBs) release copious amounts of energy across the entire electromagnetic spectrum, and so provide a window into the process of black hole formation from the collapse of massive stars. Previous early optical observations of even the most exceptional GRBs (990123 and 030329) lacked both the temporal resolution to probe the optical flash in detail and the accuracy needed to trace the transition from the prompt emission within the outflow to external shocks caused by interaction with the progenitor environment. Here we report observations of the extraordinarily bright prompt optical and  $\gamma$ -ray emission of GRB 080319B that provide diagnostics within seconds of its formation, followed by broadband observations of the afterglow decay that continued for weeks. We show that the prompt emission stems from a single physical region, implying an extremely relativistic outflow that propagates within the narrow inner core of a two-component jet.**

The GRB 080319B, discovered by NASA's Swift GRB Explorer mission<sup>1</sup> on 19 March 2008, set new records among these most luminous transient events in the Universe. GRBs are widely thought to occur through the ejection of a highly relativistic, collimated outflow (jet),

produced by a newly formed black hole. Under the standard fireball model<sup>2–6</sup>, collimated relativistic shells propagate away from the central engine, crash into each other (internal shocks) and decelerate as they plough into the surrounding medium (external/forward

<sup>1</sup>Department of Astronomy and Astrophysics, 525 Davey Laboratory, Pennsylvania State University, University Park, Pennsylvania 16802, USA. <sup>2</sup>Special Astrophysical Observatory, Nizhny Arkhizy, Zelenchukskij region, Karachai-Circassian Republic, Russia 369167. <sup>3</sup>Soltan Institute for Nuclear Studies, 05-400 Otwock-Swierk, Poland. <sup>4</sup>Centre for Astrophysics Research, University of Hertfordshire, College Lane, Hatfield AL10 9AB, UK. <sup>5</sup>Purple Mountain Observatory, Chinese Academy of Sciences, Nanjing 210008, China. <sup>6</sup>Ioffe Physico-Technical Institute, Laboratory for Experimental Astrophysics, Saint Petersburg 194021, Russian Federation. <sup>7</sup>INAF-Osservatorio Astronomico di Brera, via E. Bianchi 46, I-23807 Merate (LC), Italy. <sup>8</sup>NASA Postdoctoral Program Fellow, NSSTC, 320 Sparkman Drive, Huntsville, Alabama 35805, USA. <sup>9</sup>The UCL Mullard Space Science Laboratory, Holmbury St Mary, Surrey RH5 6NT, UK. <sup>10</sup>Astrophysics Research Institute, Liverpool John Moores University, Twelve Quays House, Birkenhead CH41 1LD, UK. <sup>11</sup>Astrophysics Science Division, Code 661, NASA's Goddard Space Flight Centre, 8800 Greenbelt Road, Greenbelt, Maryland 20771, USA. <sup>12</sup>Department of Physics and Astronomy, University of Leicester, Leicester LE1 7RH, UK. <sup>13</sup>Institute of Experimental Physics, University of Warsaw, Hoza 69, 00-681 Warsaw, Poland. <sup>14</sup>Department of Physics and Astronomy, University of Nevada Las Vegas, Las Vegas, Nevada 89154, USA. <sup>15</sup>Astrophysics Science Division, Code 660.1, NASA Goddard Space Flight Centre, 8800 Greenbelt Road, Greenbelt, Maryland 20771, USA. <sup>16</sup>Universities Space Research Association, 10211 Wincopin Circle, Suite 500, Columbia, Maryland 21044, USA. <sup>17</sup>Centre for Research and Exploration in Space Science and Technology, Code 668.8, NASA Goddard Space Flight Centre, 8800 Greenbelt Road, Greenbelt, Maryland 20771, USA. <sup>18</sup>Center for Theoretical Physics PAS, Al. Lotników 32/46, 02-668 Warsaw, Poland. <sup>19</sup>Università degli Studi di Milano Bicocca, Physics Department, Piazza della Scienza 3, I-20126 Milano, Italy. <sup>20</sup>Astronomical Institute 'Anton Pannekoek', University of Amsterdam, Kruislaan 403, 1098 SJ Amsterdam, The Netherlands. <sup>21</sup>NASA/Marshall Space Flight Center, VP62, NSSTC, 320 Sparkman Drive, Huntsville, Alabama 35805, USA. <sup>22</sup>Racah Institute for Physics, The Hebrew University, Jerusalem, 91904, Israel. <sup>23</sup>Università di Bologna, Via Ranzani 1, 40126 Bologna, Italy. <sup>24</sup>Institute for Precise Instrumentation, Nizhny Arkhizy 369167, Russian Federation. <sup>25</sup>Institute de Radioastronomie Millimétrique (IRAM), 300 rue de la Piscine, 38406 Saint Martin d'Hères, France. <sup>26</sup>Instituto de Astrofísica de Andalucía (IAA-CSIC), PO Box 03004, 18080 Granada, Spain. <sup>27</sup>INAF – Osservatorio Astronomico di Roma, via Frascati 33, 00040 Monteporzio Catone, Italy. <sup>28</sup>European Southern Observatory, Karl-Schwarzschild-Strasse 2, D-85748 Garching bei München, Germany. <sup>29</sup>INAF – Osservatorio Astronomico di Capodimonte, Salita Moiarriello, 16, 80131 Napoli, Italy. <sup>30</sup>European Southern Observatory, Casilla 19001, Santiago 19, Chile. <sup>31</sup>Space Telescope Science Institute, 3700 San Martin Drive, Baltimore, Maryland 21218, USA. <sup>32</sup>Netherlands Institute for Radio Astronomy (ASTRON), Postbus 2, 7990 AA Dwingeloo, The Netherlands. <sup>33</sup>Leiden Observatory, University of Leiden, PB 9513, Leiden 2300 RA, The Netherlands. <sup>34</sup>Centre for Astrophysics and Supercomputing, Swinburne University of Technology, Hawthorn, Victoria 3122, Australia. <sup>35</sup>Faculty of Mathematics and Physics, University of Ljubljana, Jadranska 19, SI-1000 Ljubljana, Slovenia. <sup>36</sup>Institute of Electronic Systems, Warsaw University of Technology, Nowowiejska 15/19, 00-665 Warsaw, Poland. <sup>37</sup>INAF – IAS PA, Via Ugo La Malfa 153, 90146 Palermo, Italy. <sup>38</sup>Department of Physics, University of Warwick, Coventry CV4 7AL, UK. <sup>39</sup>Aryabhata Research Institute of Observational Sciences (ARIES), Manora Peak, Nainital, Uttarakhand 263129, India. <sup>40</sup>Joint Institute for VLBI in Europe (JIVE), Postbus 2, 7990 AA Dwingeloo, The Netherlands. <sup>41</sup>ASI Science Data Center, c/o ESRIN, via G. Galilei, 00044 Frascati, Italy. <sup>42</sup>Department of Astronomy and Astrophysics, University of California, Santa Cruz, California 95064, USA. <sup>43</sup>University of Perugia, Piazza dell'Università 1, 06100 Perugia, Italy. <sup>44</sup>Physics Department, 104 Davey Laboratory, Pennsylvania State University, University Park, Pennsylvania 16801, USA.

shocks). Reverse shocks propagate back into the jet, generating optical emission. With a uniquely bright peak visual magnitude of 5.3 (Fig. 1) at a redshift of  $z = 0.937$  (ref. 7), GRB 080319B was the brightest optical burst ever observed. An observer in a dark location could have seen the prompt optical emission with the naked eye. The astronomical community has been waiting for such an event for the past nine years, ever since GRB 990123 (the previous record holder for the highest peak optical brightness) peaked at a visual magnitude of  $\sim 9$ , leading to significant insight into the GRB optical emission mechanisms<sup>8</sup>.

The location of GRB 080319B was fortuitously only  $10^\circ$  away from GRB 080319A, detected by Swift less than 30 min earlier, allowing several wide-field telescopes to detect the optical counterpart of GRB 080319B instantly. The rapid localization by Swift enabled prompt multi-wavelength follow-up observations by robotic ground-based telescopes, resulting in arguably the best broadband GRB observations obtained so far. These observations continued for weeks afterwards as we followed the fading afterglow, providing strong constraints on the physics of the explosion and its aftermath.

At its peak, GRB 080319B displayed the brightest optical and X-ray fluxes ever measured for a GRB, and one of the highest  $\gamma$ -ray fluences recorded. Our broadband data cover 11.5 orders of magnitude in wavelength, from radio to  $\gamma$ -rays, and begin (in the optical and  $\gamma$ -ray bands) before the explosion. We identify three different components responsible for the optical emission. The earliest data (at  $t \equiv T - T_0 < 50$  s) provide evidence that the bright optical and  $\gamma$ -ray emissions stem from the same physical region within the outflow. The second optical component ( $50 \text{ s} < t < 800$  s) shows the distinct characteristics of a reverse shock, and the final component

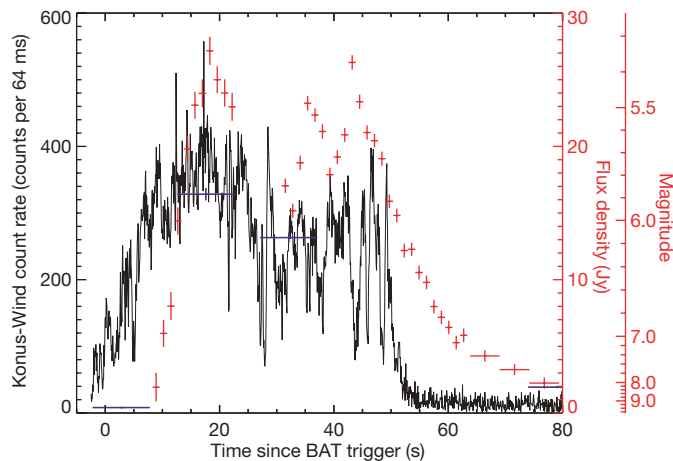


**Figure 1 | Light curve of prompt emission.** The Konus-Wind background-subtracted  $\gamma$ -ray light curve (black; 18–1,160 keV), shown relative to the trigger time  $T_0$  of the Swift-BAT. The burst had a peak  $\gamma$ -ray flux of  $F_p = (2.26 \pm 0.21) \times 10^{-5} \text{ erg cm}^{-2} \text{ s}^{-1}$ , a fluence  $F_\gamma$  (20 keV to 7 MeV) of  $(6.23 \pm 0.13) \times 10^{-4} \text{ erg cm}^{-2}$ , a peak isotropic equivalent luminosity  $L_{p,\text{iso}}$  of  $(1.01 \pm 0.09) \times 10^{53} \text{ erg s}^{-1}$  (at the luminosity distance  $d_L$  of  $1.9 \times 10^{28} \text{ cm}$ , assuming cosmological parameters  $H_0 = 71 \text{ km s}^{-1} \text{ Mpc}^{-1}$ ,  $\Omega_M = 0.27$  and  $\Omega_\Lambda = 0.73$ ), and an isotropic equivalent  $\gamma$ -ray energy release  $E_{\gamma,\text{iso}}$  of  $1.3 \times 10^{54} \text{ erg}$  (20 keV to 7 MeV). These are among the highest measured so far. Optical data from ‘Pi of the Sky’ (blue) and TORTORA (red) are superimposed for comparison. The optical emission begins within seconds of the onset of the burst. The TORTORA data have a gap during the slew of the REM telescope to this field, but show three subpeaks in the optical brightness, reaching a peak brightness of 5.3 mag (white). The  $\gamma$ -ray light curve has multiple short peaks; these are not positively correlated with the optical peaks in detail (compare with ref. 23). If the synchrotron self-absorption frequency is slightly above the optical emission, this may account for the broad optical peaks and the lack of detailed correlation. However, the optical flash begins and ends at about the same times, providing strong evidence that both originate at the same site. See Supplementary Information for a more detailed description of correlation tests. All plotted error bars are  $1\sigma$ , and quoted parameter errors are 90% confidence.

(at  $t > 800$  s) represents the afterglow produced as the external forward shock propagates into the surrounding medium. Previous measurements of GRBs have revealed one or two of these components at a time<sup>9–11</sup>, but never all three in the same burst with such clarity. GRB 080319B is therefore a testbed for broad theoretical modelling of GRBs and their environments.

### Discovery and broadband observations

Swift’s Burst Alert Telescope (BAT<sup>12</sup>; 15–350 keV) triggered<sup>13</sup> on GRB 080319B at  $T_0 = 06:12:49$  UT on 19 March 2008. The burst was detected simultaneously with the Konus  $\gamma$ -ray detector (20 keV to 15 MeV) on board the Wind satellite<sup>14,15</sup>. Both the BAT and Konus-Wind (KW) light curves (Supplementary Figs 1 and 3) show a complex, strongly energy-dependent structure, with many clearly separated pulses above 70 keV and a generally smoother behaviour at lower energies, lasting  $\sim 57$  s.

The wide-field robotic optical telescope ‘Pi of the Sky’<sup>16</sup> and the wide-field robotic instrument Telescopio Ottimizzato per la Ricerca dei Transienti Ottici Rapidi (TORTORA<sup>17</sup>) both serendipitously had the GRB within their fields of view at the time of the explosion (as they were both already observing GRB 080319A (ref. 18)). ‘Pi of the Sky’ observed the onset of the bright optical transient, which began at  $2.75 \pm 5$  s after the BAT trigger, rose rapidly, peaked at  $\sim T_0 + 18$  s and then faded below the threshold to magnitude  $\sim 12$  after 5 min. TORTORA measured the brightest portion of the optical flash with high time resolution, catching three separate peaks (Fig. 1) and enabling us to do detailed comparisons between the prompt optical and  $\gamma$ -ray emissions.

The Swift spacecraft and the Rapid Eye Mount (REM<sup>19</sup>) telescope both initiated automatic slews to the burst, resulting in optical observations with REM and the Swift Ultraviolet–Optical Telescope (UVOT<sup>20</sup>), and X-ray observations with the Swift X-ray Telescope (XRT<sup>21</sup>). Over the next several hours we obtained ultraviolet, optical and near-infrared (NIR) photometric observations of the GRB afterglow with the Swift-UVOT, REM, the Liverpool Telescope, the Faulkes Telescope North, Gemini-North, and the Very Large Telescope. Subsequent optical spectroscopy by Gemini-N and the Hobby–Eberly Telescope confirmed the redshift of 0.937 (Supplementary Figs 4 and 5). A millimetre-wavelength counterpart was detected with the IRAM Plateau de Bure Interferometer at  $\sim T_0 + 16$  h. Multiple epochs of radio observations with the Westerbork Synthesis Radio Telescope revealed a radio counterpart  $\sim 2$ –3 days after the burst. X-ray and optical observations continued for more than four weeks after the burst. The composite broadband light curves of GRB 080319B, which include all data discussed throughout this paper, and cover eight orders of magnitude in flux and more than six orders of magnitude in time, are shown in Fig. 2 and summarized in Table 1. All of these data are given in Supplementary Information.

### Ultra-relativistic prompt emission

The contemporaneous bright ‘optical flash’ and the  $\gamma$ -ray burst (Fig. 1) provide important constraints on the nature of the prompt GRB emission mechanism. Although there is a general consensus that the prompt  $\gamma$ -rays must arise from internal dissipation within the outflow, probably as a result of internal shocks, the optical flash may arise either from the same emitting region as the  $\gamma$ -rays or from the reverse shock that decelerates the outflow as it sweeps up the external medium. The reverse shock becomes important when the inertia of the swept-up external matter starts to slow down the ejecta appreciably, at a larger radius than the dissipation by internal shocks.

The temporal coincidence of the onset and overall shape of the prompt optical and  $\gamma$ -ray emissions suggest that both originate from the same physical region (see also refs 22, 23), although their respective peaks during this phase do not positively correlate in detail (see Supplementary Figs 8–10 and the related discussion in Supplementary Information). Nevertheless, the initial steep rise (at

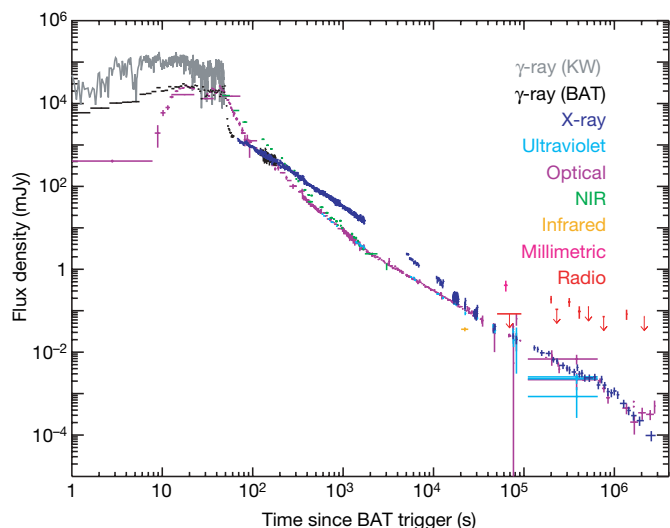


**Figure 2 | Composite light curve.** Broadband light curve of GRB 080319B, including radio, millimetric, infrared, NIR, optical, ultraviolet, X-ray and  $\gamma$ -ray flux densities. The ultraviolet, optical and NIR data are normalized to the UVOT v-band in the interval between  $T_0 + 1,500$  s and  $T_0 + 10$  ks. The Swift-BAT data are extrapolated down into the XRT bandpass (0.3–10 keV) for direct comparison with the XRT data. The combined X-ray and BAT data are scaled up by a factor of 45, and the Konus-Wind (KW) data are scaled up by a factor of  $10^4$  for comparison with the optical flux densities. This figure includes our own data, plus one VLA radio data point<sup>49</sup>, and optical data from the Katzman Automatic Imaging Telescope, Nickel and Gemini-S<sup>22</sup>. The deviations in the NIR points from  $T_0 + 100$  s to  $T_0 + 600$  s are due to strong colour evolution in the spectral energy distributions at this time; these points were not included in our overall light-curve fits (Supplementary Fig. 6). After the optical flash, the optical light curve is best described by the superposition of three different power-law components (Supplementary Fig. 6) with decay indices of  $\alpha_{\text{opt},1} = 6.5 \pm 0.9$  (the tail of the optical flash),  $\alpha_{\text{opt},2} = 2.49 \pm 0.09$  and  $\alpha_{\text{opt},3} = 1.25 \pm 0.02$ . The X-ray light curve clearly differs from the optical light curve during the first  $\sim 12$  h. After a short flat smooth transition from the tail of the  $\gamma$ -ray prompt emission, the X-ray light curve (Supplementary Fig. 7) after  $\sim 80$  s can be fitted by a triple broken power-law function with decay indices of  $1.44 \pm 0.07$ ,  $1.85 \pm 0.10$ ,  $1.17^{+0.14}_{-0.23}$  and  $2.61^{+2.04}_{-0.91}$ , and with break times of  $2,242 \pm 940$  s,  $4.1^{+2.8}_{-1.7} \times 10^4$  s and  $(1.0 \pm 0.5) \times 10^6$  s ( $\chi^2/\text{d.f.} = 880/697 = 1.26$ ), or by the superposition of two broken power-laws with decay indices of  $1.45 \pm 0.05$ ,  $2.05^{+0.44}_{-0.27}$ ,  $0.95^{+0.19}_{-0.69}$  and  $2.70^{+2.06}_{-1.12}$ , and break times of  $2,800^{+900}_{-1,400}$  s and  $9.5^{+6.2}_{-4.1} \times 10^5$  s ( $\chi^2/\text{d.f.} = 902/701 = 1.29$ ). All plotted error bars are  $1\sigma$ , and quoted parameter errors are 90% confidence.

$t < 18$  s), the rapid decline (at  $t > 43$  s) and the constant optical pulse widths indicate<sup>24–26</sup> that the optical flash did not arise from a reverse shock (compare with GRB 990123; refs 27, 28).

The flux density of the optical flash is  $\sim 10^4$  times larger than the extrapolation of the  $\gamma$ -ray spectrum into the optical band (Fig. 3). The popular interpretation of the soft  $\gamma$ -rays as synchrotron emission cannot account for such a bright optical component from the same physical region, suggesting that different radiation mechanisms must dominate in each spectral regime. The most natural (but by no means the only viable) candidates are synchrotron for the optical component and synchrotron self-Compton (SSC) for the  $\gamma$ -rays<sup>29,30</sup>. The Compton  $Y$  parameter, defined as the ratio of the inverse Compton to synchrotron energy losses, is  $Y \sim \nu F_\nu(E_p)/\nu F_\nu(E_{p,\text{syn}}) \gtrsim 10$ , where  $E_{p,\text{syn}}$  is the peak photon energy of the synchrotron  $\nu F_\nu$  spectrum, to account for the fact that the prompt  $\gamma$ -ray energy is higher than the prompt optical/ultraviolet synchrotron energy. This would imply a third spectral component arising from second-order inverse Compton scattering that peaks at energies around  $E_{p,2} \approx E_p^2/E_{p,\text{syn}} \approx 23(E_{p,\text{syn}}/20 \text{ eV})^{-1} \text{ GeV}$ . Note that the Klein–Nishina suppression becomes important only at  $E > 94(E_{p,\text{syn}}/20 \text{ eV})^{-1/2} \Gamma_3 \text{ GeV}$ , where  $\Gamma = 10^3 \Gamma_3$  is the outflow bulk Lorentz

factor. This third spectral component carries more energy than the observed  $\gamma$ -rays, by a factor  $Y \gtrsim 10$ , changing the energy budget of this burst and implying that GRB 080319B was even more powerful than inferred from the observed emission. Most of the energy in this burst was emitted in this undetected GeV component, which would have been detected by the Astro-rivelatore Gamma a Immagini Leggero (AGILE) satellite had it not been occulted by the Earth, and would have been easily detectable by the recently launched Gamma-ray Large Area Space Telescope (GLAST)<sup>31</sup> satellite.

Such bright prompt optical flashes are rare. The exceptional brightness of the optical flash in GRB 080319B implies that the self-absorption frequency  $\nu_a$  cannot be far above the optical band near the peak time. The optical brightness temperature implies that  $300 \leq \Gamma(t/3 \text{ s})^{2/3} \leq 1400$ , and therefore  $\Gamma \sim 10^3$ , where  $t_v \equiv R\Gamma^{-2}c^{-1}$  is the rough variability timescale in the internal shocks model. Because of the extremely high bulk Lorentz factor  $\Gamma$ , the internal shocks occur at an unusually large radius given by  $0.8 \leq R_{16}(t/3 \text{ s})^{1/3} \leq 20$ , where  $R_{16} = R/10^{16} \text{ cm}$ , resulting in a relatively low  $\nu_a$ , which in turn allows the optical photons to escape.

### Interpretation of the chromatic afterglow

Our broadband data set enabled us to measure the temporal and spectral evolution of GRB 080319B throughout the afterglow. After the prompt phase, the early (minutes to hours) X-ray and optical behaviour are inconsistent with the predictions of the standard afterglow theory, suggesting that they must stem from different emission regions. In particular we find that the optical, X-ray and  $\gamma$ -ray emissions from this burst are explained reasonably well by a two-component jet model<sup>32–38</sup> (Fig. 4 and Table 2), consisting of an ultra-relativistic narrow jet, surrounded by a broader jet with a lower Lorentz factor. The empirical triple broken power-law function of the X-ray light curve is then interpreted as the superposition of two broken power-law components representing these two jets (Table 2 and Supplementary Fig. 7). This structure, in which the Lorentz factor and energy per solid angle are highest near the axis and decrease outwards, either smoothly or in quasi-steps, qualitatively resembles the results of numerical simulations of jet formation in collapsars<sup>39</sup>. Further details of the model are given in Supplementary Information; here we summarize the model results and apply them to the observational data.

The optical light curve at  $50 \text{ s} < t < 800 \text{ s}$  is dominated by the second optical power-law component, which we interpret as emission from the reverse shock associated with the interaction of the wide jet with the external medium. This segment is consistent with expectations for the high-latitude emission<sup>40</sup> from a reverse shock ( $\alpha = 2 + \beta$ ) if the cooling frequency  $\nu_c$  is below the optical band and the injection frequency  $\nu_m > 10^{16} \text{ Hz}$ . Emission from the reverse shock peaks at  $t \approx 50$  s in the optical with a peak flux density of  $\sim 2\text{--}3 \text{ Jy}$ , but it is initially overwhelmed by the much brighter prompt emission and does not become visible until the latter dies away. The high peak luminosity of the optical reverse shock component soon after the end of the  $\gamma$ -ray emission indicates that the reverse shock was at least mildly relativistic. The GRB outflow could not have been highly magnetized ( $\sigma \gg 1$ ) when it crossed the reverse shock, or the reverse shock would have been suppressed<sup>41</sup>, implying that  $\sigma \lesssim 1$ , where  $\sigma$  is the ratio of electromagnetic to kinetic energy flux. However, if the outflow was too weakly magnetized ( $\sigma \ll 1$ ), the optical emission would also have been suppressed. Therefore an intermediate magnetization ( $0.1 \leq \sigma \leq 1$ ) is needed to obtain the observed bright emission from the reverse shock<sup>42,43</sup>.

In contrast, the X-ray light curve in the interval  $50 \text{ s} < t < 40 \text{ ks}$  is dominated by the forward shock of the narrow jet component interacting with a surrounding medium produced by the wind<sup>44</sup> of the progenitor star in the slow cooling case ( $\nu_m < \nu_X < \nu_c$ , where  $\nu_X$  indicates the X-ray band). The first break in the X-ray light curve is attributed to a jet break<sup>45</sup> in this narrow jet (Table 2), leading to a jet half-opening angle of  $\sim 0.2^\circ$ . Because this break is not seen in the

**Table 1 | Observations of GRB 080319B**

Facility	Epoch*	Band	Peak flux†
Swift-BAT	-120 to 182	15–350 keV	$2.3 \times 10^{-6} \text{ erg cm}^{-2} \text{ s}^{-1}$
Konus-Wind	-2 to 230	20–1,160 keV‡	$2.3 \times 10^{-5} \text{ erg cm}^{-2} \text{ s}^{-1}$
Swift-XRT	67 to $2.5 \times 10^6$	0.3–10 keV	–
'Pi of the Sky'	-1,380 to 468	White	5.9 mag
TORTORA	-20 to 97	V	5.3 mag
Swift-UVOT	68– $10^6$	White, u, v, b, uvw1, uvw2, uvm2	–
REM	51–2,070	R, I, J, H, Ks	–
Liverpool Telescope	$(1.8\text{--}2.5) \times 10^3$	SDSS r,i	–
Faulkes Telescope North	$(2.5\text{--}20.5) \times 10^4$	Bessell R,I SDSS r,i	–
Very Large Telescope	435–934	J, Ks	–
Gemini N Photometry	$3.0 \times 10^5, 4.5 \times 10^5$	r, i	–
HST	$1.6 \times 10^9$	F606W, F814W	–
Gemini N Spectroscopy	$(1.2\text{--}1.24) \times 10^4$	4,100–6,800 Å	–
Hobby–Eberly Telescope	$(2.0\text{--}2.1) \times 10^4$	4,100–10,500 Å	–
Westerbork Synthesis Radio Telescope	$(5.1\text{--}220) \times 10^4$	4.8 GHz	–
IRAM-Plateau de Bure	$(6.0\text{--}6.6) \times 10^4$	97.98 GHz	–
VLA§	$(1.98\text{--}2.02) \times 10^5$	4.86 GHz	189 $\mu\text{Jy}$
Pairitel§	$(1.27\text{--}1.77) \times 10^4$	J, H, Ks	–
KAIT§	$(0.1\text{--}1.7) \times 10^4$	Clear, B, V, I	–
Nickel§	$(0.7\text{--}2.4) \times 10^4$	B, V, R, I	–
Gemini S§	$(0.9\text{--}1.7) \times 10^5$	g, r, i, z	–
Spitzer§	$(2.20\text{--}2.24) \times 10^4$	15.8 $\mu\text{m}$	–

Details of our observations and data analysis are given in Supplementary Methods.

\* Time since BAT trigger in seconds.

† Peak fluxes listed only if a peak was actually observed.

‡ Konus-Wind light curve measured in the 20–1,160 keV range; peak flux measured in the range 20 keV to 7 MeV.

§ Observations obtained from external sources as identified in Supplementary Methods.

optical light curve, the optical flux from the forward shock of the narrow jet must be much less than that of the wide jet, implying that  $v_{\text{opt}} < v_m < v_X < v_c$  (where  $v_{\text{opt}}$  indicates the optical band).

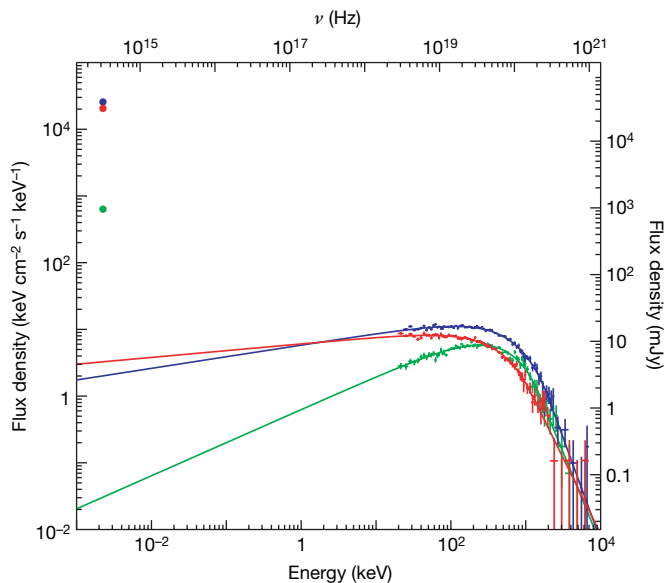


**Figure 3 | Spectral energy distribution of the prompt emission.** Konus-Wind spectra and 'Pi of the Sky' flux density in three 10-s intervals centred at  $T_0 + 3$  s (green),  $T_0 + 17$  s (blue) and  $T_0 + 32$  s (red). (Detailed time intervals and  $\gamma$ -ray spectral parameters are given in Supplementary Table 1.) The high-energy data points are from Konus-Wind, and the solid line shows the best-fit Band function<sup>50</sup> for each time interval. The time-resolved Konus-Wind spectra show that the Band-function parameters vary rapidly during the prompt emission, with the low-energy slope changing from  $-0.5$  to  $-0.9$  and  $E_p$  changing from  $\sim 740$  keV to  $\sim 540$  keV in the first 30 s (see Supplementary Table 1 and Supplementary Fig. 3). Time-resolved single power-law spectral fits of the BAT data show the photon index shifting rapidly from  $\sim 1.0$  to  $\sim 2.1$  at  $T_0 + 53$  s (near the end of the prompt phase; Supplementary Fig. 2). The low-energy points are the 'Pi of the Sky' flux density measured during about the same time interval. The optical flux density exceeds the extrapolation of the  $\gamma$ -ray model by four orders of magnitude. All plotted error bars are  $1\sigma$ .

The optical emission after  $T_0 + 800$  s is dominated by a single power-law function, which is consistent with the expectation for forward shock emission from the wide jet with  $v_m < v_{\text{opt}} < v_c$ . The late X-ray afterglow after 40 ks is also dominated by the forward shock of the wide jet with an overall spectrum of  $v_m < v_{\text{opt}} < v_c < v_X$ . At about 11 days after the burst, the X-ray light curve breaks to a steeper slope (confirmed by a late observation with the Chandra X-ray Observatory; E. Rol, personal communication). If this break is interpreted as the jet break of the wide jet (Table 2), it corresponds to an initial jet half-opening angle of  $\sim 4^\circ$ . The forward shock of the wide jet also accounts for the observed radio emission, which is strongly modulated by the effects of Galactic scintillation (see Supplementary Methods for more detailed discussion)<sup>46,47</sup> when the source is small.

Because the observed  $\gamma$ -ray emission of GRB 080319B shows very similar properties to those of most GRBs, it may be representative of the main underlying physical mechanism. If so, similar lower-energy spectral components would be expected in most GRBs. The paucity of bright optical flashes may be attributed to less relativistic outflows in most GRBs, leading to smaller emitting radii  $R$ , higher optical depths, and significantly higher values of  $v_a$ , ultimately suppressing the optical emission. In this model, the spectacular optical brightness of GRB 080318B is due mainly to its unusually large  $\Gamma$ . Previous examples of GRBs with bright optical counterparts<sup>9–11</sup> (990123, 041219a and 050820a) that also had large initial  $\Gamma$  values either lacked the high  $\gamma$ -ray luminosities or resided in a constant density and not a wind environment as with 080319B, suppressing the bright optical flash.

The afterglow may also be interpreted by alternative models such as a blast wave propagating into a complex medium (see Supplementary Figs 14 and 15 and the related discussions in Supplementary Information), or evolving microphysical parameters, but we consider the two-component jet model to be the most plausible interpretation. An interesting consequence of these theoretical considerations is that GRB 080319B, which has the best broadband data set recorded so far, is not consistent with the expectations of any of the simple GRB models previously studied. The case for multiple spectral emission components and the two-component jet presented here suggests that similar models may be able to explain at least some of the chromatic breaks seen in optical and X-ray afterglows over the

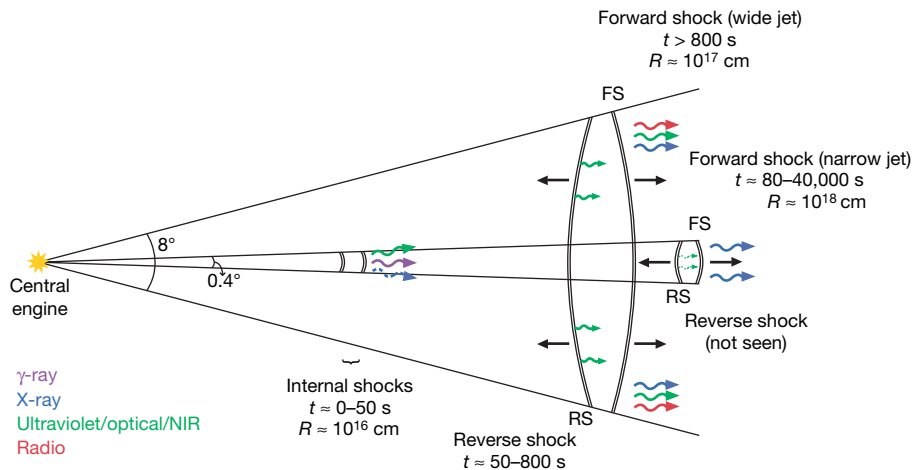


**Figure 4 | Schematic diagram of the two-component jet model.** This summary diagram shows spectral and temporal elements of our model. The prompt  $\gamma$ -ray emission is due to the internal shocks in the narrow jet, and the afterglow is a result of the forward and reverse shocks from both the narrow and wide jets. The reverse shock from the narrow jet is too faint to detect in

comparison with the bright wide-jet reverse shock and the prompt emission. If X-ray observations had begun earlier, we would have detected X-ray emission during the prompt burst. These expected (but unobserved) emission sources are indicated by the dashed photon lines. (Diagram courtesy of J. D. Myers.)

**Table 2 | Summary of two-component jet parameters**

Parameter	$\alpha_{\text{opt}}$	$\beta_{\text{opt}}$	$\alpha_x$	$\beta_x$	$p$	$v_m$	$v_c$	$t_j$ (s)	$\theta_j$ (deg)*	$E_\gamma$ (erg)
WJRS	$2.49 \pm 0.09$	$0.49 \pm 0.14$	–	–	–	$>v_{\text{opt}}; <v_x$	$<v_{\text{opt}}$	–	–	–
NJFS	–	–	$1.45 \pm 0.05; 2.05^{+0.44}_{-0.27} \ddagger$	$0.76 \pm 0.10$	2.4	$>v_{\text{opt}}; <v_x$	$>v_x; <v_\gamma$	$2,800^{+900}_{-1,400}$	0.2	$2.1 \times 10^{50}$
WJFS	$1.25 \pm 0.02$	$0.50 \pm 0.07$	$0.95 \pm 0.20; 2.70^{+2.05}_{-1.12} \ddagger$	$0.98 \pm 0.10$	2.0	$<v_{\text{opt}}$	$<v_x; >v_{\text{opt}}$	$9.5^{+6.2}_{-4.1} \times 10^5$	4.0	$1.9 \times 10^{50}$

The radiation mechanism is assumed to be synchrotron emission, as postulated in the standard fireball model<sup>2–6</sup>, and the spectral and light curve segments are fitted by power laws, described by  $F_\nu = t^{-\alpha} \nu^{-\beta}$ , with decay index  $\alpha$  and spectral energy index  $\beta$ . The details of the temporal fits are given in Fig. 2 and Supplementary Figs 6 and 7. We created broadband spectral energy distributions at 11 epochs ranging from  $T_0 + 150$  s to  $T_0 + 500$  ks. The spectral energy distributions can be fitted by power laws, broken power laws, or double broken power laws. Deviations from broken power laws at the ultraviolet and soft X-ray frequencies allow us to measure the host galaxy extinction and X-ray absorption column density (see discussion in Supplementary Information). Our resulting best-fit spectral models are described in detail in Supplementary Information and shown in Supplementary Figs 11–13. WJRS, wide-jet reverse shock; NJFS, narrow-jet forward shock; WJFS, wide-jet forward shock.

\* Half-opening angle.

‡ Post-jet break temporal slope for each jet.

past few years that have been difficult to reconcile with the standard models<sup>3,4</sup>.

The probability of being located within the tiny solid angle of the narrow jet is small ( $\sim 10^{-3}$ ). If every GRB has such a narrow jet, we should expect to detect the narrow-jet emission from a GRB every  $\sim 3$ – $10$  years. Had we observed GRB 080319B even slightly off-axis, the behaviour might have appeared similar to many other GRB afterglows. Despite the incredibly high flux and fluence of GRB 080319B, the total jet-corrected observed energy budget ( $\sim 4 \times 10^{50}$  erg) is moderate and is consistent with the overall distribution for all GRBs<sup>48</sup>. In addition, if the SSC interpretation of the prompt emission is indeed generic, it implies that a reasonably bright second-order SSC component peaking at  $\sim 10$ – $100$  GeV may be a common feature in GRBs and may significantly increase the total energy budget of a GRB. This GeV emission would be seen with a delay of a few seconds compared with the optical emission. GLAST will soon test these predictions.

Received 11 May; accepted 11 July 2008.

- Gehrels, N. et al. The Swift gamma-ray burst mission. *Astrophys. J.* **611**, L1005–L1020 (2004).
- Rees, M. J. & Mészáros, P. Relativistic fireballs—energy conversion and time-scales. *Mon. Not. R. Astron. Soc.* **258**, 41–43 (1992).
- Mészáros, P. & Rees, M. J. Optical and long-wavelength afterglow from gamma-ray bursts. *Astrophys. J.* **476**, 232–237 (1997).
- Wijers, R. A. M. J., Rees, M. J. & Mészáros, P. Shocked by GRB 970228: the afterglow of a cosmological fireball. *Mon. Not. R. Astron. Soc.* **288**, 51–56 (1997).
- Zhang, B. & Mészáros, P. Gamma-ray bursts: progress, problems and prospects. *Int. J. Mod. Phys. A* **19**, 2385–2472 (2004).
- Sari, R., Piran, T. & Narayan, R. Spectra and light curves of gamma-ray burst afterglows. *Astrophys. J.* **497**, L17–L20 (1998).
- Vreeswijk, P. M. et al. VLT/UVES redshift of GRB 080319B. *GCN Circ.* **7444** (2008).

- Castro-Tirado, A. J. et al. Decay of the GRB 990123 optical afterglow: implications for the fireball model. *Science* **283**, 2069–2073 (1999).
- Akerlof, C. et al. Observation of contemporaneous optical radiation from a  $\gamma$ -ray burst. *Nature* **398**, 400–402 (1999).
- Blake, C. H. et al. An infrared flash contemporaneous with the  $\gamma$ -rays of GRB 041219a. *Nature* **435**, 181–184 (2005).
- Vestrand, W. T. et al. A link between prompt optical and prompt  $\gamma$ -ray emission in  $\gamma$ -ray bursts. *Nature* **435**, 178–180 (2005).
- Barthelmy, S. D. et al. The Burst Alert Telescope (BAT) on the SWIFT Midex Mission. *Space Sci. Rev.* **120**, 143–164 (2005).
- Racusin, J. L. et al. GRB 080319B: Swift detection of an intense burst with a bright optical counterpart. *GCN Circ.* **7427** (2008).
- Golenetskii, S. et al. Konus-Wind observation of GRB 080319B. *GCN Circ.* **7482** (2008).
- Aptekar, R. L. et al. Konus-W Gamma-Ray Burst Experiment for the GGS Wind Spacecraft. *Space Sci. Rev.* **71**, 265–272 (1995).
- Cwiok, M. et al. Search for GRB related prompt optical emission and other fast varying objects with ‘Pi of the Sky’ detector. *Astrophys. Space Sci.* **309**, 531–535 (2007).
- Molinari, E. et al. TORTOREM: Two-telescope complex for detection and investigation of optical transients. *Nuovo Cimento B* **121**, 1525–1526 (2006).
- Pagani, C. et al. Swift observation of GRB 080319A. *GCN Rep.* **121**, (2008).
- Zerbi, F. M. et al. The REM telescope: detecting the near infra-red counterparts of gamma-ray bursts and the prompt behavior of their optical continuum. *Astron. Nachr.* **322**, 275–285 (2001).
- Roming, P. W. A. et al. The Swift Ultra-Violet/Optical Telescope. *Space Sci. Rev.* **120**, 95–142 (2005).
- Burrows, D. B. et al. The Swift X-Ray Telescope. *Space Sci. Rev.* **120**, 164–195 (2005).
- Bloom, J. et al. Observations of the naked-eye GRB 080319B: implications of nature’s brightest explosion. Preprint at (<http://arxiv.org/abs/0803.3215>) (2008).
- Kumar, P. & Panaitescu, A. What did we learn from gamma-ray burst 080319B? Preprint at (<http://arxiv.org/abs/0805.0144>) (2008).
- Kobayashi, S. Light curves of gamma-ray burst optical flashes. *Astrophys. J.* **545**, 807–812 (2000).
- Nakar, E. & Piran, T. Early afterglow emission from a reverse shock as a diagnostic tool for gamma-ray burst outflows. *Mon. Not. R. Astron. Soc.* **353**, 647–653 (2004).

26. Ramirez-Ruiz, E. & Fenimore, E. E. Pulse width evolution in gamma-ray bursts: evidence for internal shocks. *Astrophys. J.* **539**, 712–717 (2000).
27. Sari, R. & Piran, T. GRB 990123: The optical flash and the fireball model. *Astrophys. J.* **517**, L109–L112 (1999).
28. Mészáros, P. & Rees, M. J. GRB 990123: reverse and internal shock flashes and late afterglow behaviour. *Mon. Not. R. Astron. Soc.* **306**, 39–43 (1999).
29. Panaitescu, A. & Mészáros, P. Gamma-ray bursts from upscattered self-absorbed synchrotron emission. *Astrophys. J.* **544**, L17–L21 (2000).
30. Kumar, P. & McMahon, E. A general scheme for modelling  $\gamma$ -ray burst prompt emission. *Mon. Not. R. Astron. Soc.* **384**, 33–63 (2008).
31. Steinle, H. *et al.* Measurements of gamma-ray bursts from upscattered self-absorbed synchrotron emission. *Chinese J. Astron. Astrophys.* **6** (Suppl. S1), 365–368 (2006).
32. Pedersen, H. *et al.* Evidence for diverse optical emission from gamma-ray burst sources. *Astrophys. J.* **496**, 311–315 (1998).
33. Frail, D. *et al.* The enigmatic radio afterglow of GRB 991216. *Astrophys. J.* **538**, L129–L132 (2000).
34. Ramirez-Ruiz, E., Celotti, A. & Rees, M. J. Events in the life of a cocoon surrounding a light, collapsar jet. *Mon. Not. R. Astron. Soc.* **337**, 1349–1356 (2002).
35. Kumar, P. & Piran, T. Energetics and luminosity function of gamma-ray bursts. *Astrophys. J.* **535**, 152–157 (2000).
36. Peng, F., Königl, A. & Granot, J. Two component jet models of gamma-ray burst sources. *Astrophys. J.* **626**, 966–977 (2005).
37. Berger, E. *et al.* A common origin for cosmic explosions inferred from calorimetry of GRB030329. *Nature* **426**, 154–157 (2003).
38. Huang, Y. F. *et al.* Rebrightening of XRF 030723: further evidence for a two-component jet in a gamma-ray burst. *Astrophys. J.* **605**, 300–306 (2004).
39. Zhang, W., Woosley, S. E. & MacFadyen, A. I. Relativistic jets in collapsars. *Astrophys. J.* **586**, 356–371 (2003).
40. Kumar, P. & Panaitescu, A. Afterglow emission from naked gamma-ray bursts. *Astrophys. J.* **541**, L51–L54 (2000).
41. Zhang, B. & Kobayashi, S. Gamma-ray burst early afterglows: reverse shock emission from an arbitrarily magnetized ejecta. *Astrophys. J.* **628**, 315–334 (2005).
42. Zhang, B., Kobayashi, S. & Mészáros, P. Gamma-ray burst early optical afterglows: implications for the initial Lorentz factor and the central engine. *Astrophys. J.* **595**, 950–954 (2003).
43. Kumar, P. & Panaitescu, A. A unified treatment of the gamma-ray burst 021211 and its afterglow. *Mon. Not. R. Astron. Soc.* **346**, 905–914 (2003).
44. Chevalier, R. A. & Li, Z. Y. Wind interaction models for gamma-ray burst afterglows: the case for two types of progenitors. *Astrophys. J.* **536**, 195–212 (2000).
45. Sari, R., Piran, T. & Halpern, J. Jets in gamma-ray bursts. *Astrophys. J.* **519**, L17–L20 (1999).
46. Cordes, J. M. & Lazio, T. J. W. NE2001.1. A new model for the galactic distribution of free electrons and its fluctuations. Preprint at ([http://arxiv.org/PS\\_cache/astro-ph/pdf/0207/0207156v3.pdf](http://arxiv.org/PS_cache/astro-ph/pdf/0207/0207156v3.pdf)) (2002).
47. Walker, M. A. Interstellar scintillation of compact extragalactic radio sources. *Mon. Not. R. Astron. Soc.* **294**, 307–311 (1998).
48. Frail, D. *et al.* Beaming in gamma-ray bursts: evidence for a standard energy reservoir. *Astrophys. J.* **562**, L55–L58 (2001).
49. Soderberg, A. *et al.* Radio detection of GRB 080319B. *GCN Circ.* **7506** (2008).
50. Band, D. *et al.* BATSE observations of gamma-ray burst spectra. I. Spectral diversity. *Astrophys. J.* **413**, 281–292 (1993).

**Supplementary Information** is linked to the online version of the paper at [www.nature.com/nature](http://www.nature.com/nature).

**Acknowledgements** We thank E. Rol for comments. This research was supported by NASA, the National Science Foundation (NSF), the Agenzia Spaziale Italiana, the Ministero dell'Università e della Ricerca (MUR), the Ministero degli Affari Esteri, the Netherlands Organization for Scientific Research (NWO), the National Science Foundation of China, the Russian Space Agency, Science and Technology and Facilities Council (STFC), the Slovenian Research Agency, the Ministry for Higher Education, Science, and Technology, Slovenia, and the Polish Ministry of Science and Higher Education.

**Author Information** Reprints and permissions information is available at [www.nature.com/reprints](http://www.nature.com/reprints). Correspondence and requests for materials should be addressed to J.L.R. ([racusin@astro.psu.edu](mailto:racusin@astro.psu.edu)).